Shear stress on the structure control of supported fly ash-based catalyst and its application in SCR denitration

Shu Hao
Xi'an University of Technology
Liu Yuling (lyl29992359@163.com)
Xi'an University of Technology
Jia Yang
Xi'an University of Technology
Bai Fang
Key Laboratory of Green Process and Engineering

Research Article

Keywords: Shear stress, Mn-Ce/FA, Catalyst, Selective catalytic reduction, Solid waste resource utilization

Posted Date: March 16th, 2021

DOI: https://doi.org/10.21203/rs.3.rs-236182/v1

Abstract

In order to control NOx in flue gas, reduce the preparation cost of denitration catalyst. In this paper, solid waste fly ash is used as a catalyst carrier, a shear reactor is used to prepare Mn-Ce/FA catalyst, and it is successfully applied to SCR denitration. The catalyst was characterized and analyzed by SEM, XRD, FTIR, XPS. The results show that the catalyst prepared by shearing has more dispersed active components. The catalyst prepared at power of 80 W, time of 20 min, rotation speed of 120 r/min, and the active component Mn-Ce molar ratio is 1:1. The denitration performance is the best, up to 82.6% within 30 min. The introduction of SO 2 still showed high catalytic activity and stability, and the removal rate of NO was reduced to 73.21%. After the introduction of SO 2 was stopped, the removal rate rebounded to 77.89%.

1. Introduction

With the rapid development of social economy and industry, NO_X emissions have gradually increased, which has brought serious harm to the natural environment and human life and production (Meng et al. 2018). According to statistics, the annual global NO_X emissions are about 50 million tons or more, and my country is a fossil fuel-based country (Qi et al. 2020), of which more than 95% of anthropogenic NO_X emissions come from the combustion process of fossil fuels (Rahman et al. 2019). Therefore, it is essential for the removal of NO_X.

SCR (Selective Catalytic Reduction) is the most widely used denitration method at home and abroad at this stage (Vita et al. 2018). This method can make the removal efficiency of nitrogen oxides reach more than 90%. The basic principle of SCR technology is that the reducing agent ($NH_3 \cdot H_2O$) is used to contact the NO_X pollutants in the flue gas under the catalysis of the catalyst (Zhang et al. 2020; Zhang et al. 2021). After the reaction, the NO_X can be reduced to finally generate harmless N_2 to achieve the purpose of removing NO_X.

In order to avoid catalyst poisoning caused by high concentrations of dust and SO_2, SCR equipment is generally installed downstream of electrostatic precipitators and desulfurization devices, which makes the flue gas temperature usually lower than 270 ℃ (Najafpoo et al. 2018; Li et al. 2020). Therefore, the development of SCR catalysts that are active at low temperatures (150-270 ℃) has significance. The structure, type, morphology, composition and related parameters of the catalyst can directly affect the denitration performance, so choosing the appropriate catalyst is the core of the flue gas denitration process. The catalyst is mainly composed of carrier and active components (Jaegers et al. 2019; Jablonska et al. 2018; Italiano et al. 2016). The current industrial denitration catalyst is mainly vanadium-titanium (V_2O_5 -WO_3/TiO_2), which has the disadvantages of higher cost and narrow reaction temperature range (Felix et al. 2020). If it can be replaced by cheap materials and can be used for low-temperature denitration, the cost of denitration will be greatly reduced.

Fly ash refers to the particulate matter captured from the flue gas after coal combustion, and is the main solid waste discharged from coal-fired power plants. As an important coal by-product, fly ash is mainly

composed of Al_2O_3 and SiO_2 (Qin et al. 2019; Kechagia et al. 2021; Czuma et al. 2020). Fly ash has a wide range of sources and has certain physical properties. It is gradually being used in the field of flue gas denitration (Chen et al. 2017). Fly ash as a carrier and compounded with other substances as a denitration carrier has been studied by a large number of scholars in recent years. When fly ash is used as a carrier for denitration without modification, the denitration efficiency is relatively low, mainly due to the lack of effective active components (Chen et al. 2014; Gan et al. 2021). Fly ash shows better denitration activity after being loaded with metal active components. The performance of fly ash denitration catalyst is mainly affected by conditions such as active components and catalyst preparation methods (Chen et al. 2021). The active component is the main reaction site in the catalytic process of the catalyst, which plays a key role in the electron transfer and the absorption and desorption of the reaction component (Ren et al. 2020). Metals and metal oxides are currently commonly used active components for denitration. In the denitration reaction, metal electrons match or transfer NO electrons to oxidize NO to NO_2, which will aggravate the denitration process of the catalyst (Yan et al. 2020; Wahiduzzaman et al. 2018; Vogel et al. 2020). Therefore, the characteristics of metal oxides can greatly aggravate the denitration catalytic reaction.

The preparation method of the catalyst is very important for the subsequent catalytic effect of the catalyst. The active component forms and distribution modes of the catalysts prepared by different methods are different, which leads to the change of the catalytic effect (Veerapandian et al. 2019; Selvamani et al. 2017; Schroeder l et al. 2020). At present, denitration catalysts mainly load active components on fly ash carriers through impregnation and precipitation methods (Zhou et al. 2021). These two preparation methods can embed the active components on the carrier in different forms to produce a catalytic effect. However, the common problems of these two methods are the uneven loading of active components, the loading does not meet the calculation standard, the long impregnation and roasting time, and the complicated process (Wang et al. 2021).

The classical model theory of shear force studies the nucleation process of catalysts from the perspective of thermodynamic instability. Experiments show that the bubble core in the critical state grows into a stable bubble through thermodynamic diffusion, and the shear effect of the flow field also promotes the transition from the critical bubble core to a stable bubble (Gholami et al. 2020). The key to shear stress is the conversion of mechanical shear energy to free energy at the bubble interface. The concept of shear energy was first proposed by S.T.Lee. In his study of continuous extrusion foaming experiments containing nucleating agents, he pointed out that it is not that the shear rate alone has an effect on the nucleation of bubbles, but Shearing stress plays a major role, and the product of shearing area and shearing distance constitutes the work done by shearing. A large number of studies have found that refining the dispersed agglomerates through external shear force is beneficial to the significant improvement of the catalyst structure and performance (Dadi et al. 2021).

Therefore, the paper uses solid waste fly ash as the catalyst carrier, metal oxides as the active component, and a high-shear reactor to systematically study the critical conditions for the clustering of shear-aggregated fly ash-based catalysts, and propose an induced shear catalyst contribution

mechanism of forming and shear power, shear rate, and shear time to catalyst synthesis, and applying them to industrial boiler flue gas denitration. It not only improves the atmospheric environment to a certain extent, but also realizes the resource utilization of solid waste.

2. Experimental

2.1. Material synthesis

2.1.1 Fly ash molding

Mix fly ash and calcium bentonite at a ratio of 4:1, add 20 wt% deionized water to form agglomerates, put them into the catalyst molding extrusion device, extrude them, and place them in a 105 ℃ electric blast drying oven 1 h, get the columnar fly ash carrier.

2.1.2 Preparation of Mn-Ce/FA catalyst by shear loading

Weigh appropriate amount of manganese nitrate (0.04 mol), weigh appropriate amount of cerium nitrate according to different Mn-Ce ratios, and configure it into a 50 mL manganese nitrate-cerium nitrate mixed solution, weigh 8 g of fly ash carrier into the shearing reactor. Mn-Ce/FA catalysts with different ratios were prepared under certain shear speed, shear power and shear time. Put the prepared Mn-Ce/FA catalyst into a muffle furnace at 500 °C for 4 h and then grind and siev to 40-60 mesh.

2.2 Catalyst evaluation device

The activity evaluation of the catalyst was carried out in a vertical denitration experimental device. Simulated gas was introduced to observe the changes of its NO data. As shown in Fig. 1.

SCR operating conditions: reaction temperature 220 ℃, total gas flow 200 mL/min, O_2 concentration 6%, NO: 500PPM, NH_3: 500PPM, SO_2: 500PPM, remaining gas is filled with N_2, and Testo340 (flue gas analyzer) is used in the experiment The NO concentration in the flue gas at the outlet of the experiment is detected, and the activity of the catalyst is evaluated by the NO conversion rate. The calculation formula of the conversion rate is as follows:

$$\text{Removal efficiency} = \frac{C_{NO_{inlet}} - C_{NO_{outlet}}}{C_{NO_{inlet}}} \times 100\% \qquad \text{Eq. (1)}$$

2.3 Characterization

SEM: Using secondary electron signal imaging to capture the characteristics of the sample surface, that is, scanning the sample with a particularly narrow electron beam, so that the two interact and produce an effect. The secondary electrons can magnify the topography of the sample surface, which appears to be

established in chronological order when scanning the sample (that is, obtained by point-by-point imaging). The SEM model in this article is JSM-6460LV (produced by JEOL Ltd.).

XRD: Use X-ray diffraction to analyze the internal spatial distribution of substances. That is: when X-rays of a certain wavelength are irradiated to a crystalline substance, the regularly arranged atoms (or ions) scatter the X-rays, so that certain phases are strengthened, and a unique diffraction phenomenon occurs. The samples in this article have been tested by XD-3 X-ray diffraction analyzer (produced by Beijing Puxi General Instrument Co., Ltd.) to obtain XRD patterns. The test conditions of the sample are: Cu, Kα rays, tube voltage 36 kV, tube current 25 mA, 2θ is 10°-80°, scanning rate 4 (°)/min.

FTIR: The compound can be accurately identified and the molecular structure of the substance can be determined. He can not only quantitatively analyze single components and individual components in the mixture, but also quantitatively analyze samples that are difficult to separate or have no obvious characteristic peaks. The Fourier infrared spectrometer used in this article was produced by Bruker and the model is VERTEX 70.

XPS: XPS is an important tool for analyzing the surface structure and composition of elements. The principle is: After the sample is irradiated by X-rays, the inner electrons (or valence electrons) in atoms (or molecules) are excited. Photons can excite photoelectrons (measurable energy), and the composition of the object to be measured can be obtained through the photoelectron spectrogram (that is, the abscissa is the kinetic energy of the photon, and the ordinate is the relative intensity (pulse/s)). The model of the X-ray photoelectron spectrometer used in this article is: ESCALAB250 (produced by Thermo Fisher Scientific, USA). The energy resolution of the instrument is 0.45 eV (Ag), the sensitivity is 180 KCPS, and the image resolution is 3 μm. The analysis results are all corrected with C1s.

3. Results And Discussion

3.1 Study on Mn-Ce/FA catalyst for denitration and sulfur resistance

When preparing the metal-supported catalyst in this paper, based on the previous research results of the research group, the loading amount of Mn is selected as 5%, and the high-shear reactor is used for structural control, and different shearing speed, shearing power, shearing time and different Mn-Ce molar ratio is an influence on the performance of flue gas denitration, and the results are shown in Fig. 2.

Fig. 2(a) is a study of the effect of different shearing time on the performance of the catalyst. It can be seen that the shearing time is 20 min, the denitration efficiency is the best, and the denitration effect is as high as 82.6% within 30 min. When the shearing time is short, the reaction between fly ash and active components is insufficient, making it impossible to completely decompose. Moreover, the short-term shear does not have enough etching effect on the catalyst surface, and the pores blocked by the nitrate solution cannot be completely opened. With the extension of the shearing time, the surface etching effect becomes more and more sufficient, the nitrate can be fully decomposed, and a uniformly distributed pore structure is formed. But when the shearing time is too long, the smaller pore structure that has been

synthesized uniformly is continuously sheared and disappeared, and the small pore structure is directly sheared to form large pores and reduce the active sites. Therefore, when the shear time is 20 min, the denitration performance is the best.

Fig. 2(b) is a study of the effect of different shearing speeds on the performance of the catalyst. It can be seen that the effect is best when the shearing speed is 150 r/min, and the denitration effect is as high as 82.6% within 30 min. The reason is that when the shearing speed is low, the fly ash in the reactor cannot be lifted up completely, the work generated is small, and a good shearing effect cannot be obtained. When the shearing speed is increased to a certain level, the particles are under the action of mechanical force, most of the fly ash and nitrate solution are lifted from the bottom to a certain height, the relative shearing speed is relatively large, the dispersion kinetic energy of the particles further increases, and the active component on the surface of fly ash is more even. When the shearing speed is too high, the particle dispersion kinetic energy rises to a large amount, and the particles become very fine, which increases the number of surface atoms of the particles, and the surface atom coordination number is insufficient, the surface energy increases, the molecules are abnormally active, and the particles appear agglomeration. Therefore, when the shearing speed is 150 r/min, the denitration performance is the best.

Fig. 2(c) is a study of the effect of different shearing power on the performance of the catalyst. It can be seen that the effect is best when the shearing power is 80 W, and the denitration effect is as high as 82.6% within 30 min. The reason is that when the power is small, the cavitation effect of shear is small, the mechanical collision force between the nitrate solution and the fly ash is not enough, the reaction is not sufficient, and the active components are unevenly loaded and dispersed on the fly ash. However, when the power is too large, it will have a certain inhibitory effect on the combination of nitrate solution and fly ash, and then affect the denitration performance of blast furnace slag. Therefore, when the shearing power is 80 w, the denitration performance is optimal.

Fig. 2(d) is a study of the effect of different Mn-Ce molar ratios on the performance of the catalyst. It can be seen that the denitration effect of the bimetal supported catalyst is significantly increased. When cerium element and manganese element act together, metallic cerium is easy to generate Ce^{3+}/Ce^{4+} redox couple, and unstable oxygen vacancy and oxygen migration. It shows excellent oxygen storage-release capacity and unique redox performance. Obviously make up for the shortage of the narrow reaction window of manganese metal. When the ratio of Mn-Ce is 1:1, the denitration effect is as high as 82.6% within 30 min. When the Mn-Ce ratio is low, the active components are not enough to be uniformly distributed on the surface of the catalyst, and fewer active sites are formed. With the increase of the loading molar ratio, the optimal loading ratio of manganese and cerium gradually reaches saturation, so that they can exert their respective functions to a greater extent and have a synergistic effect to increase the denitration effect of the catalyst. However, when the loading ratio is too high, the metal cerium oxide completely covers the metal manganese. During the shearing process, the manganese nitrate is not fully decomposed, and the active sites of the formed manganese oxide are insufficient, resulting in the denitration reaction in the process, the complementary effects of manganese and cerium are inhibited,

the catalytic reaction is insufficient, and the denitration effect is not ideal. Therefore, when the Mn-Ce molar ratio is 1:1, the catalyst has excellent catalytic activity and the best denitration performance.

Fig. 2(e) shows the stability evaluation experiment of the Mn-Ce/FA catalyst under the condition of SO_2. It can be seen from the figure that in the SCR process without SO_2, the Mn-Ce/FA catalyst can maintain high efficiency in the removal rate of NO. When 500ppm SO_2 is introduced, the activity of the catalyst is affected, and the removal rate of NO was reduced to 73.21%. After the SO_2 was stopped, the removal rate rebounded to 77.89%. The reason is that SO_2 and the reactant (NH_3 or NO) may have a competitive adsorption relationship. These results indicate that the Mn-Ce/FA catalyst exhibits a higher NO removal rate and good stability under the condition of SO_2.

3.2 Characterization

3.2.1 SEM

Fig. 3 is the SEM of the Mn-Ce/FA catalyst after denitration and sulfur resistance, 3(a) is Mn-Ce/FA (fresh), 3(b) is after denitration, and 3(c) is after sulfur resistance. It can be seen that the gaps between the catalyst particles after denitration are reduced, and there is a phenomenon of particle agglomeration on the surface of the catalyst. The reason is that the ammonium sulfate produced during the SCR reaction gathers on the surface of the catalyst, reducing the gaps between the particles. The pore structure of the catalyst reduces the denitration performance of the catalyst and deactivates it. After a certain amount of SO_2 is introduced into the system, the reduction of the pore structure of the catalyst surface is more obvious. The main reason is that SO_2 reacts with the catalyst, resulting in a reduction of active sites on the catalyst surface.

3.2.2 XRD

Fig. 4 is the XRD pattern of FA, Mn/FA, Mn-Ce/FA after denitration and sulfur resistance. It can be seen that when only Mn is loaded, the catalyst does not show the diffraction peak of manganese, indicating that the manganese oxide is evenly distributed on the surface of the catalyst, and the manganese mainly exists in the form of amorphous. The active components in the catalyst are mainly Mn_3O_4 and Mn_2O_3 crystal phases. When Ce is introduced, the crystal form of the catalyst changes significantly, and the characteristic peaks of Mn_3O_4 and Mn_2O_3 are weakened, indicating that the addition of CeO_X can reduce the content of bottom valence Mn in MnOx. Compared with loaded Mn, there are more CeO_2 peaks at 27°. This is a solid solution with a fluorite structure formed by CeO_2 and Mn_2O_3, which is also called a mantou peak (Appaturi et al. 2021). The rest of the diffraction peaks are obviously broadened, which indicates that the addition of Ce will reduce the degree of crystallization of the catalyst and promote the conversion of the active components in the catalyst from the crystalline phase to the amorphous phase, which is very beneficial to the catalytic reaction. The analysis of the Mn-Ce/FA catalyst before and after denitration and sulfur resistance showed that the solid solution of Mn-Ce structure disappeared, which indicated that the Mn-Ce solid solution was the active substance of the catalyst mainly involved in the

reaction. After the sulfur resistance, a new peak occurred. It is the characteristic peak of CeO_2. At the same time, no characteristic peak of sulfate is found. The reason may be that it is highly dispersed on the surface of the catalyst and does not reach the detection limit of XRD.

3.2.3 FT-IR

Fig. 5 shows the FTIR of the Mn-Ce/Fa catalyst after denitration and sulfur resistance. It can be seen that the 3400 cm^{-1} stretch vibration peak attributable to the free -OH- on the surface of the fly ash, or the water physically adsorbed on the sample surface, However, the preparation process of the catalyst has passed the drying process, and the possibility of vibration sealing of water molecules is relatively small. Near 2925-2848 cm^{-1} is the symmetrical and antisymmetric stretching vibration bands of CH_2 and CH_3. 2335 cm^{-1} appeared C≡C and C≡N stretching vibration peaks. 1589 cm^{-1} is attributed to the adsorption peak of carbon-based functional groups. 1465 cm^{-1} is the stretching vibration peak of H-C-H. 1387 cm^{-1} is the symmetrical shear vibration δC-H(s) of $-CH_3$, and its intensity is very weak, indicating that the number of $-CH_3$ is very small. 1345 cm^{-1} is C-H bending vibration. 1100 cm^{-1} is the antisymmetric stretching vibration peak of Si-O-Si, the raw material of fly ash. 1036 cm^{-1} is the C-O stretching vibration. 400-900 cm^{-1} is the characteristic peak of metal oxide decoration and manganese. 560 cm^{-1} is the symmetrical stretching vibration peak of O-Si-O in the silicon-oxygen tetrahedron, and it is also the 6-coordinated Al-O vibration. These stretching vibration peaks are all related to the important component of mullite in fly ash.

3.2.4 XPS

In order to study the element morphology of the catalyst surface, XPS characterization was performed on the Mn-Ce/FA catalyst, as shown in Fig. 6. The electron binding energy spectra of the corresponding Ce3d, Mn2p, O1s orbitals are shown in Fig. 6(a).

Fig. 6(b) is the XPS spectrum of the O1s orbital of the catalyst, which mainly includes two peaks, corresponding to the surface lattice oxygen and chemisorption oxygen respectively. Among them, lattice oxygen (O_β) appears at 529.3-530.0 eV, and chemically adsorbed oxygen (O_α) appears at 531.2-531.9 eV. Using XPSpeak41 to perform peak fitting integration on the O spectra, the relative concentrations of O_α and O_β, namely O_α/O_β, were 9.64, 6.71, 3.37, respectively. When the catalyst participates in the reaction, the chemical adsorbed oxygen is relatively active and plays a major role in the oxidation reaction, which can promote the reaction of NO and O_2 to produce NO_2, and then the SCR reaction will occur. After denitration and sulfur resistance, the relative concentration of O_α decreased from 9.64 to 3.37, indicating that O_α participated in the reaction and was consumed in the process.

Fig. 6(c) shows the XPS spectrum of the Mn2p orbital of the catalyst. The Mn2p orbital contains two main peaks. The $Mn2p_{3/2}$ orbital appears at 642 eV and the $Mn2p_{1/2}$ orbital appears at 654eV. Corresponding to the mixed valence state where Mn^{3+} and Mn^{4+} coexist, Mn^{4+} accounts for a larger proportion. The peak splitting results of $Mn2p_{3/2}$ using XPS peak software are shown in the figure.

Among them, the vicinity of 641.1, 642.3, and 644.1 eV are Mn^{2+}, Mn^{3+} and Mn^{4+} respectively. The greater the ratio of Mn^{4+}/Mn^{3+}, the stronger the activity of the catalyst, so it can be seen that the fresh catalyst prepared has the strongest denitration activity. The ratio of Mn^{4+}/Mn^{3+} of the catalyst after sulfur resistance is larger than that after denitration. The reason is that SO_2 forms competitive adsorption with reactants through intermolecular forces on the catalyst surface, and the content of reducing agent in the reaction system is consumed, which slows the conversion of NOx to N_2 in the process of redox electron transfer. Therefore, the content of high-valence compounds contained in the metal oxide will be higher.

Fig. 6(d) shows the XPS spectrum of the Ce3d orbital of the catalyst. The XPS spectrum of Ce3d orbital is more complicated. Among them, the peaks of u_1-u_6 correspond to Ce^{4+}, and the two peaks of v_1, v_2 are assigned to Ce^{3+} ions. Studies have shown that the presence of Ce^{3+} will cause more chemisorption oxygen to accumulate on the surface of the catalyst, while the presence of Ce^{4+} on the catalyst surface will form more lattice oxygen. When Ce^{3+} and Ce^{4+} are present on the catalyst, the two valence states will mutually transform to form oxygen vacancies. It is beneficial to the improvement of the catalytic activity of the catalyst. Ce is mainly based on Ce^{4+}. After denitration and after sulfur resistance, Ce^{3+} gradually decreases, and Ce^{4+} gradually increases. The mutual transformation of the two promotes denitration. At the same time, the oxidability of Ce^{4+} can change the valence of Mn and improve the activity of the catalyst. The addition of the co-activator Ce can improve the oxidation-reduction ability of the catalyst, and interact with the multivalent Mn to generate electron transfer. The Ce^{4+}/Ce^{3+} ratio increased after sulfur resistance, because the introduction of SO_2 would increase the acidic sites on the catalyst surface and increase the catalyst activity.

4 Conclusion

This paper uses industrial solid waste fly ash as the catalyst carrier. The bimetallic Mn-Ce/FA catalyst was prepared under different shear modification conditions, and its denitration performance and sulfur resistance were studied. FT-IR, XRD, XPS and SEM characterization methods were used to analyze the catalyst to determine the morphology, structure and properties of the catalyst. The results show:

(1) For the catalyst prepared under shearing action, the active components are more uniformly dispersed on the catalyst surface, and the catalytic activity is excellent.

(2) The catalyst prepared under a shear time of 20 min, a power of 80 W and a speed of 120 r/min has excellent structure and good performance. Under the optimal shear conditions, when the Mn-Ce molar ratio is 1:1, the catalyst has strong stability, strong denitration performance, and certain sulfur resistance.

(3) Mn-Ce/FA catalyst is applied to flue gas denitration, which not only realizes the recycling of solid waste, but also has certain significance for atmospheric environmental protection.

Declarations

Credit authorship contribution statement

Conceptualization, Shu Hao; Methodology, Liu Yuling; Software, Jia Yang; Validation, Shu Hao; Investigation, Shu Hao; Data Curation, Jia Yang; Writing-Original Draft Preparation, Jia Yang and Bai Fang; Writing-Review & Editing, Shu Hao.

Data availability All data generated or analyses during this study are included in this published article.

Compliance with ethical standards

Competing interests: The authors declare no competing financial interest.

Ethics approval: Not applicable

Consent to participate: Not applicable

Consent to publish: Not applicable

Funding

This work is supported by the National Natural Science Foundation of China [51578452]; Key R & D Program in Shaanxi Province [2020SF-354]; Open Fund of Shaanxi Key Laboratory of Geological Support for Coal Green Exploitation [NO. DZBZ2020-08].

References

Appaturi J.N, Ramalingam R.J, Al-Lohedan H.A, Khoerunnisa F, Ling T.C, Ng E.P (2021) Selective synthesis of dioxolane biofuel additive via acetalization of glycerol and furfural enhanced by MCM-41-alanine bifunctional catalyst. Fuel 288: 119573. https://doi.org/10.1016/j.fuel.2020.119573.

Chen J.Y, Fu P, Lv D.F, Chen Y, Fan M.L, Wu J.L, Meshram A, Mu B, Li X, Xia Q.B (2021) Unusual positive effect of SO_2 on Mn-Ce mixed-oxide catalyst for the SCR reaction of NOx with NH_3. Chem Eng J 407: 127071. https://doi.org/10.1016/j.cej.2020.127071.

Chen M, Jin L.S, Liu Y.H, Guo X.R, Chu J.W (2014) Decomposition of NO in automobile exhaust by plasma–photocatalysis synergy. Environ Sci Pollut R 21 1242-1247. https://doi.org/10.1007/s11356-013-2021-2.

Chen M.Y, Zhao M.M, Tang F.S, Ruan L, Yang H.B, Li N (2017) Effect of Ce doping into V_2O_5-WO_3/TiO_2 catalysts on the selective catalytic reduction of NOx by NH. J Rare Earth 35 1206-1215. https://doi.org/10.1016/j.jre.2017.06.004.

Czuma N, Zarebska K, Motak M, Galvez M.E, Da Costa P (2020) Ni/zeolite X derived from fly ash as catalysts for CO_2 methanation. Fuel 267 117139. https://doi.org/10.1016/j.fuel.2020.117139.

Dadi R.K, Daya R, Kumar A, Joshi S.Y, An H.M, Cunningham M.J, Currier N.W, Yezerets A (2021) A modeling and experimental study on hydrothermal aging deactivation of NO oxidation activity on Pt-Pd catalyst. Appl Catal B-Environ 283 119655. https://doi.org/10.1016/j.apcatb.2020.119655.

Felix D, Murgulet D (2020) Nitrate isotopic composition of sequential Hurricane Harvey wet deposition: Low latitude NOx sources and oxidation chemistry. Atmos Environ 238 117748. https://doi.org/10.1016/j.atmosenv.2020.117748.

Gan L.N, Li K.Z, Niu H.J.Y, Peng Y, Chen J.J, Huang Y.D, Li J.H (2021) Simultaneous removal of NOx and chlorobenzene on V_2O_5/TiO_2 granular catalyst: Kinetic study and performance prediction. Front Env Sci Eng 15 70. https://doi.org/10.1007/s11783-020-1363-5.

Gholami F, Gholami Z, Tomas M, Vavrunkova V, Mirzaei S, Vakili M (2020) O-2 over M@La-Fe/AC (M = Mn Ce) Catalyst. Catalysts 10 1322. https://doi.org/10.3390/catal10111322.

Italiano C, Balzarotti R, Vita A, Latorrata S, Fabiano C, Pino L, Cristiani C (2016) Preparation of structured catalysts with Ni and Ni Rh/CeO_2 catalytic layers for syngas production by biogas reforming processes. Catal Today 273 3-11. https://doi.org/10.1016/j.cattod.2016.01.037.

Jablonska M, Wolkenar B, Beale A.M, Pischinger S, Palkovits R (2018) Comparison of Cu-Mg-Al-O-x and Cu/Al_2O_3 in selective catalytic oxidation of ammonia (NH_3-SCO). Catal Commun 110 5-9. https://doi.org/10.1016/j.catcom.2018.03.003.

Jaegers N.R, Lai J.K, He Y, Walter E, Dixon D.A, Vasiliu M, Chen Y, Wang C.M, Hu M.Y, Mueller K.T, Wachs I.E, Wang Y, Hu J.Z (2019) Mechanism by which Tungsten oxide promotes the activity of supported V_2O_5/TiO_2 catalysts for NO_X abatement: structural effects revealed by V-51 MAS NMR spectroscopy. Angew Chem Int Edit 58 12609-12616. https://doi.org/10.1002/anie.201904503.

Kechagia P, Koutroumpi D, Bartzas G, Peppas A, Samouhos M, Deligiannis S, Tsakiridis P.E (2021) Waste marble dust and recycled glass valorization in the production of ternary blended cements. Sci Total Environ 761 143224. https://doi.org/10.1016/j.scitotenv.2020.143224.

Li S, Gong H.Y, Hu H.Y, Liu H.M, Huang Y.D, Fu B, Wang L.L, Yao H (2020) Re-using of coal-fired fly ash for arsenic vapors in-situ retention before SCR catalyst: Experiments and mechanisms. Chemosphere 254 126700. https://doi.org/10.1016/j.chemosphere.2020.126700.

Meng D.M, Xu Q, Jiao Y.L, Guo Y, Guo Y.L, Wang L, Lu G.Z, Zhan W.C (2018) Spinel structured CoaMnbOx mixed oxide catalyst for the selective catalytic reduction of NOx with NH_3. Appl Catal B-Environ 221 652-663. https://doi.org/10.1016/j.apcatb.2017.09.034.

Najafpoo A.A, Jafari A.J, Hosseinzadeh A, Jazani R.K, Bargozin H (2018) Optimization of non-thermal plasma efficiency in the simultaneous elimination of benzene toluene ethyl-benzene and xylene from

polluted airstreams using response surface methodology. Environ Sci Pollut R 25 233-241. https://doi.org/10.1007/s11356-017-0373-8.

Qi Y.F, Shan X.W, Wang M.T, Hu D.D, Song Y.B, Ge P.L, Wu J (2020) Study on Low-Temperature SCR Denitration Mechanisms of Manganese-Based Catalysts with Different Carriers. Water Air Soil Poll 231 289. https://doi.org/10.1007/s11270-020-04644-5.

Qin L, Gao X.J, Li Q.Y (2019) Influences of coal fly ash containing ammonium salts on properties of cement paste. J Environ Manage 249 109374. https://doi.org/10.1016/j.jenvman.2019.109374.

Rahman M, Rooney R, Hara K, Nakatani S (2019) Measurement of automobile NO from bag and continuous stream by quantum cascade laser spectroscopy. Int J Engine Res 20 261-273. https://doi.org/10.1177/1468087417750937.

Ren Z.X, Zhang H.L, Wang G.Y, Pan Y.C, Yu Z.W, Long H.M (2020) Effect of Calcination Temperature on the Activation Performance and Reaction Mechanism of Ce-Mn-Ru/TiO_2 Catalysts for Selective Catalytic Reduction of NO with NH_3. Acs Omega 5 33357-33371. https://doi.org/10.1021/acsomega.0c05194.

Schroeder C, Schroeder W, Yang S,S, Nystrom A, Cai Z, Subramanian S, Li S.J, Gundersen M.A, Cronin S.B (2020) Plasma-enhanced NOx remediation using nanosecond pulsed discharges in a water aerosol matrix. Fuel Process Technol 208 106521. https://doi.org/10.1016/j.fuproc.2020.106521.

Selvamani A, Shanthi K, Santhanaraj D, Babu C.M, Srinivasan V.V, Thirukumaran P, Ramkumar V, Shakilaparveen A, Balasubramanian R (2017) Effective removal of automobile exhausts over flower-like Ce1-xCuxO_2 nanocatalysts exposed active {100} plane. J Rare Earth 36 603-612. https://doi.org/10.1016/j.jre.2017.12.006.

Veerapandian S.K.P, Ye Z.P, Giraudon J.M, De Geyter N, Morent R, Lamonier J.F (2019) A plasma assisted Cu-Mn mixed oxide catalysts for trichloroethylene abatement in moist air. J Hazard Mater 379 120781. https://doi.org/10.1016/j.jhazmat.2019.120781.

Vita A, Italiano C, Ashraf M.A, Pino L, Specchia S (2018) Syngas production by steam and oxy-steam reforming of biogas on monolith-supported CeO_2-based catalysts. Int J Hydrogen Energ 43 11731-11744. https://doi.org/10.1016/j.ijhydene.2017.11.140.

Vogel D.J, Lee Z.R, Hanson C.A, Henkelis S.E, Smith C.M, Nenoff T.M, Dixon D.A, Rimsza J.M (2020) Predictive Acid Gas Adsorption in Rare Earth DOBDC Metal-Organic Frameworks via Complementary Cluster and Periodic Structure Models. J Phys Chem C 124 26801-26813. https://doi.org/10.1021/acs.jpcc.0c08282

Wahiduzzaman M, Lenzen D, Maurin G, Stock N, Wharmby M.T (2018) Rietveld Refinement of MIL-160 and Its Structural Flexibility Upon H_2O and N-2 Adsorption. Eur J Inorg Chem 32 3626-3632. https://doi.org/10.1002/ejic.201800323.

Wang B, Yang F, Song Z.J, Sun L.S (2021) Removal of Hg-0 NO and SO_2 by the surface dielectric barrier discharge coupled with Mn/Ce/Ti-based catalyst. Environ Sci Pollut R. https://doi.org/10.1007/s11356-020-11886-7.

Yan Q.H, Hou X.T, Liu G.C, Li Y.R, Zhu T.Y, Xin Y.J, Wang Q (2020) Recent advances in layered double hydroxides (LDHs) derived catalysts for selective catalytic reduction of NOx with NH_3. J Hazard Mater 400 123260. https://doi.org/10.1016/j.jhazmat.2020.123260.

Zhang L, Shu H, Jia Y, Lei Z, Bai F, Kuang W, Qi L.B, Shang J, Chao Wei (2021) Study on denitration and sulfur removal performance of Mn-Ce supported fly ash catalyst. Chemosphere 128646. https://doi.org/10.1016/j.chemosphere.2020.1286.

Zhang L, Shu H, Jia Y, Lei Z, Xu D (2020) Study on Solid Waste Pyrolysis Coke Catalyst for Catalytic Cracking of Coal Tar. Int J Hydrogen Energ 45 19280-19290. https://doi.org/10.1016/j.ijhydene.2020.05.075.

Zhou C.X, Zhang H.L, Zhang Z, Li L.M (2021) Improved reactivity for toluene oxidation on MnOx/CeO2-ZrO2 catalyst by the synthesis of cubic-tetragonal interfaces. Appl Surf Sci 539 148188. https://doi.org/10.1016/j.apsusc.2020.148188.

Figures

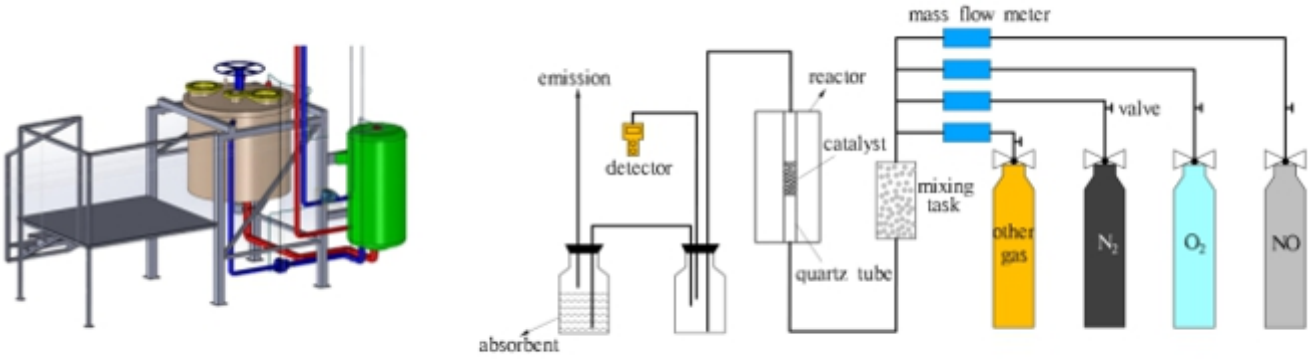

Figure 1

Catalyst evaluation device

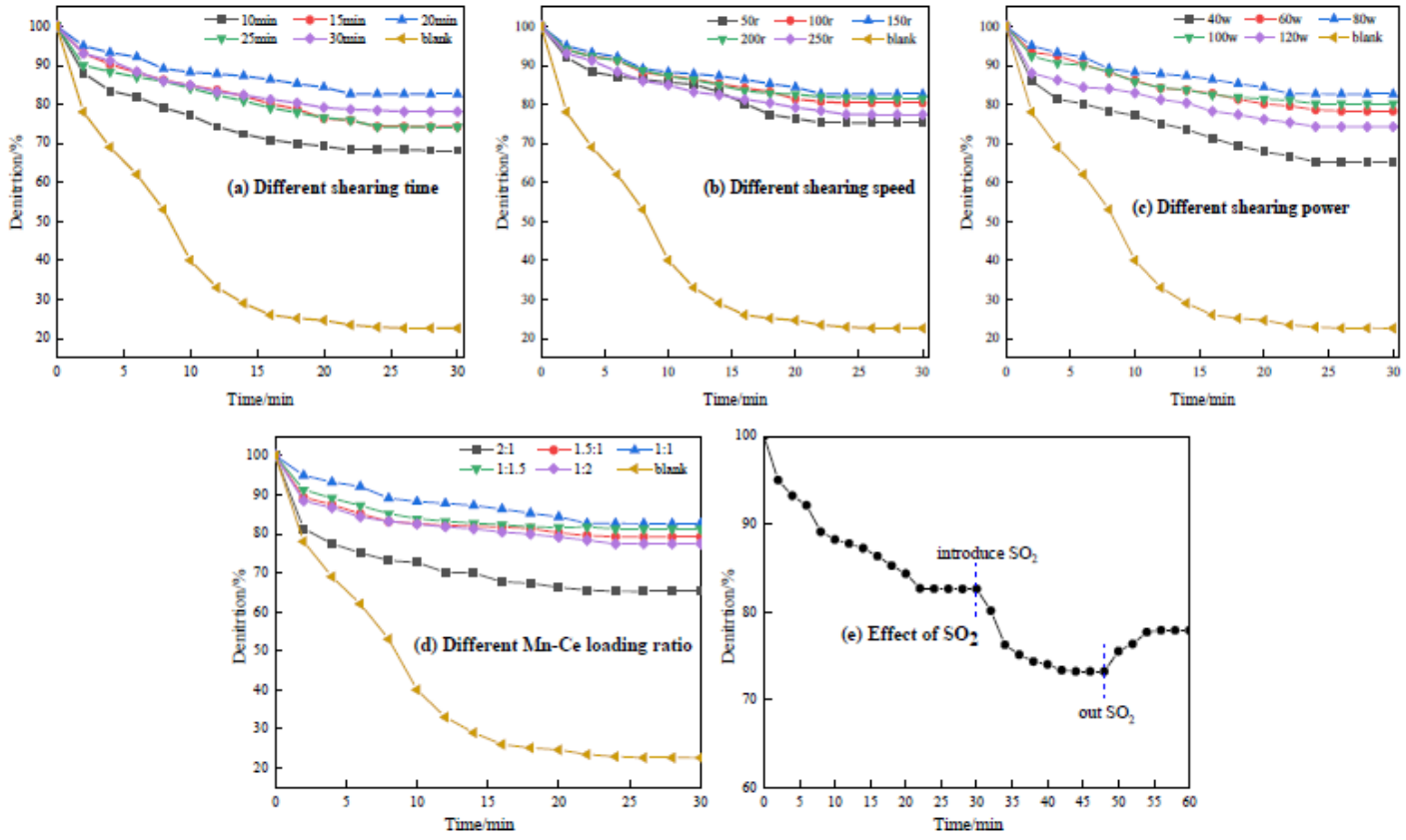

Figure 2

Mn-Ce/FA catalyst for denitration and sulfur resistance

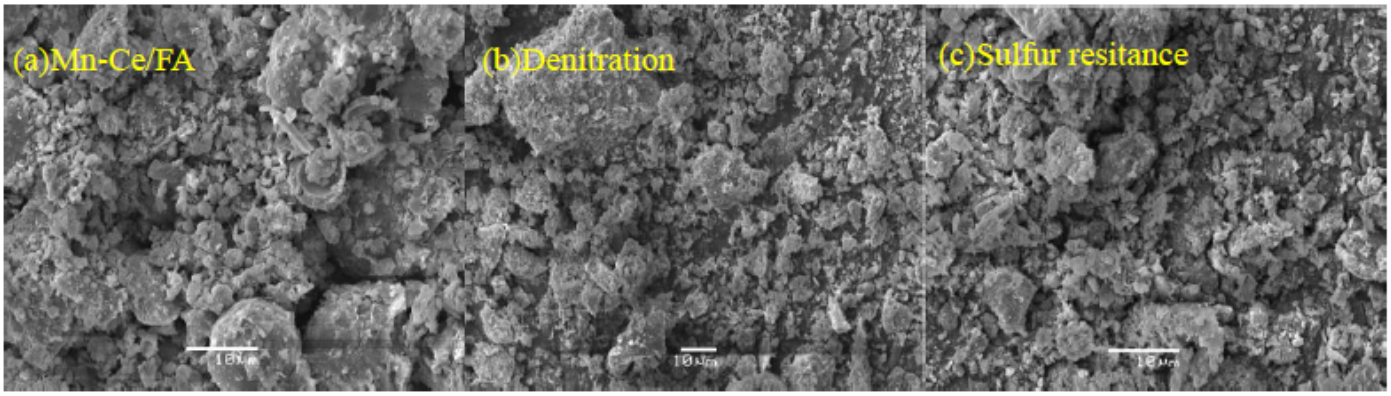

Figure 3

SEM of Mn-Ce/FA

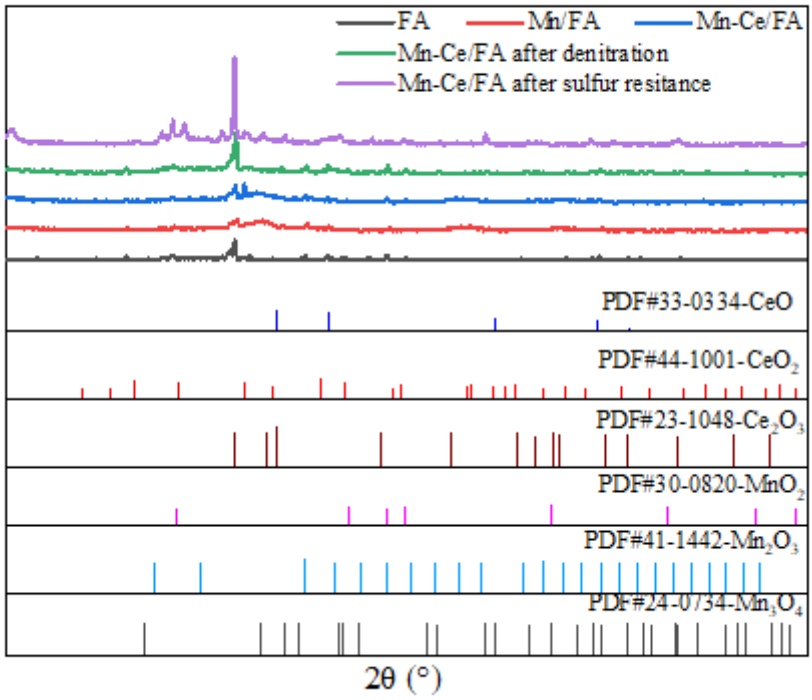

Figure 4

XRD of Mn-Ce/FA

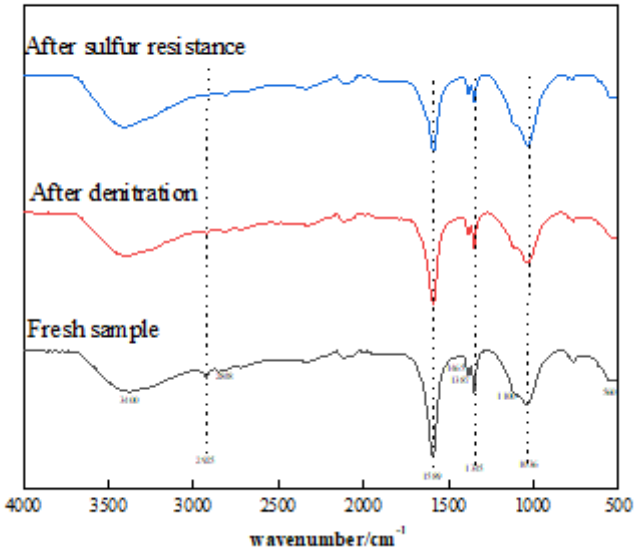

Figure 5

FTIR of Mn-Ce/FA

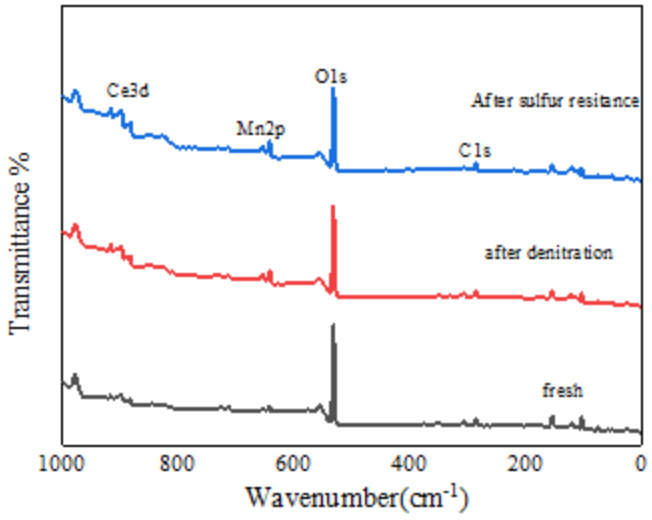

(a) Full spectrum

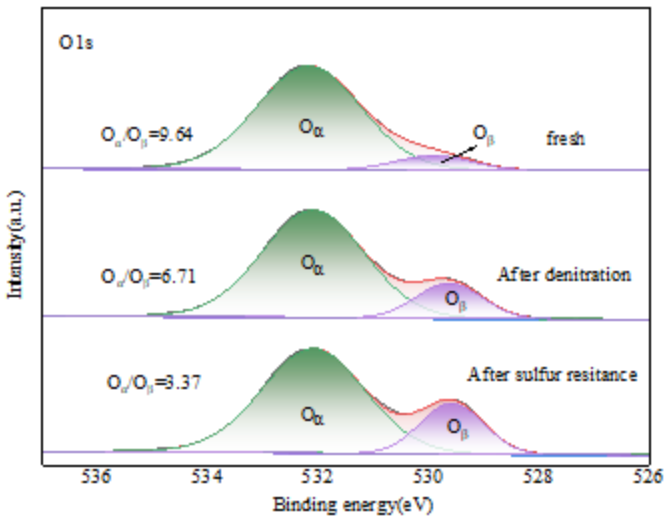

(b) XPS spectrum of the O1s

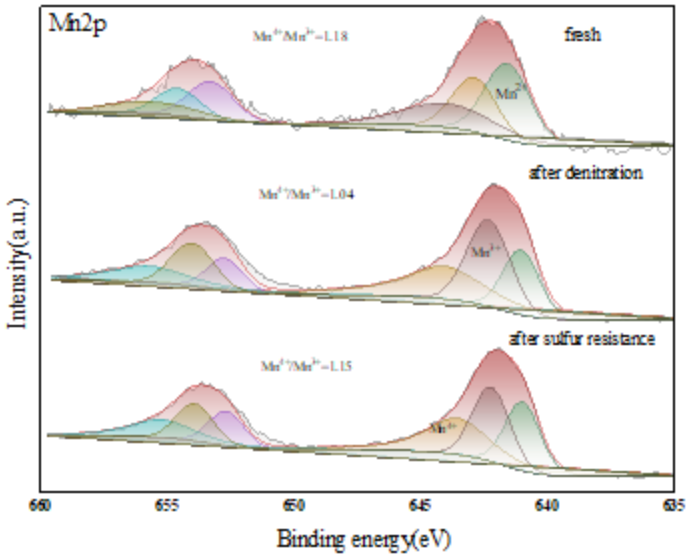

(c) XPS spectrum of the Mn2p

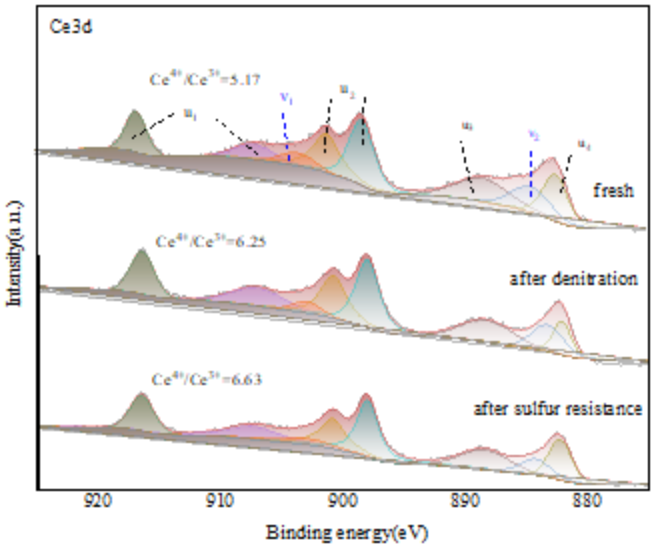

(d) XPS spectrum of the Ce3d

Figure 6

XPS of Mn-Ce/FA

Supplementary Files

This is a list of supplementary files associated with this preprint. Click to download.

- Highlights.doc
- GraphicalAbstract.pdf